The Influence of Talc as a Nucleation Agent on the Nonisothermal Crystallization and Morphology of Isotactic Polypropylene: The Application of the Lauritzen–Hoffmann, Avrami, and Ozawa Theories

Nikola Kocic, Karsten Kretschmer, Martin Bastian, Peter Heidemeyer

SKZ—Das Kunststoff-Zentrum, Würzburg, Deutschland

Received 12 October 2011; accepted 24 January 2012
DOI 10.1002/app.36880
Published online in Wiley Online Library (wileyonlinelibrary.com).

ABSTRACT: A new method is proposed, which can be used to analyze the influence of different additives and fillers on the nonisothermal crystallization of polymers. The composites of talc in isotactic polypropylene (i-PP) were prepared using a corotating twin-screw extruder. The compounds were subsequently dried and injection molded. PP morphology and talc dispersion were visualized using optical microscopy and computed tomography. Wide-angle X-ray scattering and small-angle X-ray scattering measurements provided an insight into the crystal structure of PP. The data obtained from nonisothermal DSC measurements were fitted to the Avrami model for the nonisothermal case. The calculated Avrami's exponent (n), which takes into account the influence of talc on the nucleation and growth of the PP crystals, was used in the combination of Lauritzen–Hoffman and Ozawa models to calculate the nucleation parameter (K_g). A good agreement was found between the model predictions and literature values. The examination shows that the developed model extension gives an expected trend in the case of i-PP filled with talcs from the same origin but with different particle sizes. Furthermore, it is shown that delaminated talc with a higher specific surface is more efficient in nucleation of i-PP. Thus, the introduced model extension could be a useful tool for comparing of nucleation ability of different additives in the crystallization of polymers. © 2012 Wiley Periodicals, Inc. J Appl Polym Sci 000: 000–000, 2012

Key words: crystallization; morphology; modeling; composites; thermoplastics

INTRODUCTION

Thermoplastic materials are increasingly used in industrial production. This counts especially for semicrystalline polymers, such as polyethylene, polypropylene (PP), or polyamide. The tertiary structure (supermolecular structure) of isotactic PP is relatively complicated. PP crystallizes in different crystal forms.[1] The degree of crystallinity as well as crystal form, structure, and orientation of the crystal unit (lamellae and spherulite) varies widely due to changes in the PP structure[1–5] or the processing parameters.[1,6,7] The introduction of a second component into PP further modifies the thermodynamics and kinetics of the crystallization process, which, as a consequence, further changes the morphology, quantity, and orientation of the PP crystal phase.[5,8–13] These changes in morphology can drastically alter physical properties, such as transparency, impact strength, Young's modulus, yield stress, or elongation at brake.[3,5,14–19] Consequently, nucleation agents are used to achieve some desirable properties or to decrease the cycle times during injection molding.

Pure talc (hydrated magnesium silicate) is often used as filler in the plastic industry. A large amount of the talc used is mixed with PP. This is due to the different properties of the compound, which depend on the structure of PP, the properties, dimensions, and concentration of talc.[20] It is a known fact that talc has a strong nucleating effect on PP. Fujiyama and Wakino,[21] for example, observed a slight increase in crystallinity for composites with 0.5 wt % of talc compared to pure PP. Ferrage et al.[12] examined several types of talc (talcs from China, Spain, Italy, Gabon, and Brazil) as nucleation agents. From wide-angle X-ray scattering (WAXS) experiments, they concluded (similar to Denac et al.[22]) that talc is a strong α-nucleation agent in the case of PP and showed that the crystallization of PP on talc particles has an epitaxial relationship characterized by a strong orientation of PP chains. To characterize the nucleation effect of talc, they used an onset of crystallization temperature ($T_{c,\text{onset}}$), determined from nonisothermal DSC measurements and intensity ratio between (040) and (110) reflections of α-form of isotactic polypropylene (i-PP), measured with WAXS. They found a good correlation between $T_{c,\text{onset}}$

Correspondence to: N. Kocic (n.kocic@skz.de).

and both $I(110)/I(040)$ and particle size d_{50} and concluded that the presence of talc particles in the concentration of 0.5 wt % causes the crystallization to be complete after only 50 min, compared to 2 h for pure PP. They believed that talc particle size is the principal factor affecting the crystallization of PP, where the talc samples with the finest particles sizes are more efficient as nucleation agent in the case of PP. Pukánszky und Móczó[13] showed that talc is a stronger nucleation agent than calcium carbonate in respect to PP. The change in the vol % of talc from 0 to 30% produces the increase of the crystallization peak temperature from 117 to $\sim$ 135°C and the change in the heat of fusion (i.e., degree of crystallinity) from 103 to 114 J/g.

Isothermal crystallization of polymers has been widely examined.[23] The Avrami macrokinetic model has been used to analyze the overall kinetics of crystallization[4,24,25]:

$$X(t) = 1 - \exp\lfloor -Kt^n \rfloor \tag{1}$$

where $X(t)$ is the relative degree of crystallinity as a function of time, defined as

$$X(t) = \frac{\int_0^t \frac{dH}{dt}\,dt}{\int_0^{t\_\text{end}} \frac{dH}{dt}\,dt} \tag{2}$$

In eq. (2), dH denotes the measured enthalpy of crystallization during an infinitesimal time interval dt. The limits t and t_{end} are used to denote the elapsed time during the crystallization and at the end of the process, respectively. Avrami's exponent (n) and Avrami's rate constant (K) are constants specific to a given crystalline morphology and type of nucleation for particular crystallization conditions.[26] The double logarithmic form of eq. (1) is used to fit the experimental data:

$$\log[-\ln(1 - X(t))] = \log K + n \cdot \log t \tag{3}$$

If the model adequately represents the process, the plot of the left-hand side of the eq. (3) versus log t should be a straight line, with the Avrami's exponent n as the slope and log K as the intercept. The Avrami model is made under the assumption of unimpeded spherical crystal growth and complete crystallization.[24,27] Because of this, it represents the initial portions of polymer crystallization correctly, but for the later stages of crystallization, it deviates from the experimental data.[4] Some authors used the Avrami approach for the case of nonisothermal crystallization.[24,28,29] However, it should be pointed out that when it comes to nonisothermal crystallization, the Avrami parameters K and n do not have the same physical meaning, as when speaking about isothermal crystallization.[30]

The Avrami equation provides useful data on the overall kinetics of crystallization, but gives little insight into the molecular organization of the crystalline regions, the structure of the spherulite, etc.[4]

Isothermal polymer crystallization can also be analyzed using the spherulitic growth rate [$G(T)$] in the context of the Lauritzen–Hoffman theory,[31] which is made under the assumption of regular, adjacent reentry folding, and a kinetically controlled nucleation process.[4,23] Concerning this approach, the growth rate G is given as a function of the crystallization temperature T by the following biexponential equation:

$$G(T) = G_0 \exp\left[\frac{-U}{R(T - T_\infty)}\right] \exp\left[\frac{-K_g}{T\Delta T}\right] \tag{4}$$

where G_0 is the pre-exponential factor, which accounts for the factors that affect the transport of macromolecular chains toward the growing site, U is the activation energy for the transport of polymer segments to the site of crystallization, T_∞ is the theoretical temperature at which all motion associated with viscous flow or reptation ceases and is defined as $T_\infty = T_g - 30$, T_g is the glass transition temperature, K_g is the nucleation parameter, which denotes the energy required for the formation of a nucleus of a critical size (in K^2), ΔT denotes the supercooling (equal to $T^0_m - T$), whereby T^0_m is the equilibrium melting temperature and R is the universal gas constant. The values of G_0, U, and K_g are not temperature dependent. The first exponential term in eq. (4) contains the contribution of the diffusion process, while the second exponential term represents the contribution of the nucleation process to the spherulitic growth rate. The nucleation parameter (K_g) can be calculated from

$$K_g = \frac{\zeta \sigma \sigma_e b_0 T^0_m}{k_b \Delta H_f} \tag{5}$$

where ζ is the parameter of the mode of nucleation (four in case of heterogeneous nucleation,[27] that is, regime 3^4), σ and σ_e are the side surface (lateral) and fold surface-free energies, which measure the work required to create a new surface, b_0 is the single layer thickness, ΔH_f is the enthalpy of the melting of an ideal crystal, and k_b is the Boltzmann constant. When it comes to isothermal crystallization, the nucleation parameter K_g can be calculated from eq. (4) using the logarithmic transformation:

$$\ln(G(T)) + \frac{U}{R(T - T_\infty)} = \ln(G_0) - \frac{K_g}{T\Delta T} \tag{6}$$

If the left side of the eq. (6) is plotted against $1/(T\Delta T)$, a straight line with the slope K_g should be obtained, when the model adequately represents the process.

As opposed to isothermal crystallization, only a few models have been developed to explain nonisothermal crystallization.[30] The reason behind this is the cooling rate, which could further complicate the situation. However, isothermal measurements are often restricted to a narrow crystallization temperature range, because the response time of the measuring system must be small compared to the overall crystallization time.[32] The actual processing is also often nonisothermal in nature.[28,25] Hence, examinations under nonisothermal conditions are a useful complement in order to understand the crystallization of polymers during the process. The Model developed by Ozawa[33] is used for the nonisothermal crystallization under a constant cooling rate. In the development of this model, it is assumed that crystals originate from the nuclei and expand as spheres. According to Ozawa, the nonisothermal crystallization process can be divided into an infinite number of small isothermal crystallization steps, with the radial growth rate being constant at any given step. In this manner, the untransformed fraction of polymer at temperature T can be calculated as follows:

$$1 - X(T) = \exp\left[\frac{-g\int_{T_m^0}^{T} N(\theta)[R(T) - R(\theta)]^m G(\theta)d\theta}{\alpha^n}\right] \quad (7)$$

where $X(T)$ denotes the relative degree of crystallinity as a function of temperature, $N(\theta)$ is the number of nuclei per unit volume activated between T_m^0 and θ, $G(\theta)$ is the radial growth rate at a given temperature θ, α is the cooling rate ($\alpha = dT/dt$), g represents the factors that depend on the dimension of the growth, and n is Ozawa's exponent, which is related to, but different from the Avrami exponent[34] and is equal to $m + 1$ for the instantaneous, that is, $m + 2$ for the sporadic nucleation, respectively. Factors g and m are given in Table I.

Functions $X(T)$ and $R(Q)$ are given by

$$X(T) = \frac{\int_0^T \frac{dH}{dT}dT}{\int_0^{T\_\text{end}} \frac{dH}{dT}dT} \quad (8)$$

and

$$R(T) = \int_{T_m^0}^{T} G(\theta)d\theta; \quad (9)$$

TABLE I
Factors g and m Concerning the Dimension of Crystall Growth, Used in Ozawa's Equation

Dimension of growth	m	g
One-dimensional growth	0	Area of the nuclei
Two-dimensional growth	1	2π
Three-dimensional growth	2	3π

Monasse and Haudin[32] proposed an extension of Ozawa's theory to predict the nucleation parameter (K_g) under nonisothermal conditions. Through appropriate combination and mathematical transformations of eqs. (4) and (7), they obtained the following equation:

$$\frac{2}{3}\ln[-\ln(1 - X(T))] - \ln\left(-\frac{d(\ln(1 - X(T)))}{dT}\right) - \frac{U}{R(T - T_\infty)} = C + \frac{K_g}{T(T_m^0 - T)} \quad (10)$$

where C is a constant. As regards pure PP, they plotted experimental values on the left-hand side of the eq. (10) against $1/(T_m^0 - T)$ and obtained K_g as the slope.

In this article, we used the nonisothermal DSC measurements and a newly proposed extension of the Monasse–Haudin approach to calculate and discuss the influence of talc as a nucleation agent in the crystallization of i-PP. To quantify the effect of different talc concentrations on the nucleation of i-PP, we calculated the nucleation parameter (K_g) for every talc concentration. The influence of talc particle size as well as talc specific surface on K_g was also examined using the proposed model extension.

EXPERIMENTAL

Materials

PP HD120MO, which is 95% isotactic, with an M_w = 365 kg/mol, M_w/M_n = 5.4,[35] and a melt flow index (MFI) of 8 g/10 min at 230°C/2.16 kg was kindly supplied by Borealis. This grade of PP is not nucleated, does not contain antistatic agents, and contains an antioxidant package based on phosphites/phenolics and a stearate-based acid scavenger. Fintalc M05SLC was kindly supplied by Mondo Minerals and was used as filler for the basic study. To discuss the influence of talc particle size on K_g, we used Fintalc M10 E, Fintalc M15 E, and Fintalc M30 SL, also supplied by Mondo Minerals. Two other talc types (Jetfine 8CF and Luzenac HAR T84) from Luzenac were used for investigating the influence of the specific surface of talc particles with the same origin and particle size on the crystallization of i-PP. The main properties of the talc types

TABLE II
The Main Properties of the Talc Used (Manufacturer Data)

Talc type	d_{50} (μm)	Top cut (μm)	Specific surface BET (m^2/g)
Fintalc M05SLC	2.3	10[a]	9.5
Fintalc M10E	2.8	13[a]	8
Fintalc M15E	4.2	14[a]	6.5
Fintalc M30SL	10	27[a]	3.5
Jetfine 8CF	2	5.7[b]	8
Luzenac HAR T84	2	11.3[b]	16

[a] d_{98}.
[b] d_{95}.

used are summarized in Table II. Neither of the talc types is surface-coated. All materials were used as received.

Composite preparation

All composites were prepared by melt mixing on a Leistritz (model ZSE 18 Hpe) corotating twin-screw extruder ($L = 810$ mm, $D = 18$ mm) with a temperature profile of 225, 225, 225, 215, 215, 210, 210, and 205°C (die), screw speed of 240 min^{-1}, and throughput of 6 kg/h (torque was between 80 and 90%). Along the screws, there were appropriate screw elements in order to introduce polymer melting and particle fine dispersion in the polymer melt. The process parameters were adjusted to obtain the smallest possible degradation of PP and held constant afterward. As a rough sign of the amount of degradation, the MFI was used. The difference in MFI between compounded and as-received pellets without filler for the acceptable temperature profile in extruder was 1 g/10 min (at 230°C/2.16 kg). To check if the proposed talc concentrations were reached, an annealing of compounded granulate was carried out at 600°C for 3.5 h, and the results are shown in Figure 1.

As shown, the difference between the desired and obtained talc concentrations during compounding was in all cases less than 0.35% and can therefore be neglected.

After compounding, the pellets were air dried at 80°C for 45 min in a drying chamber and injection molded using the Battenfeld Unilog 4000 machine, with barrel temperatures of 200, 205, 210, and 215°C (die), a mold temperature of 25°C, an injection rate of 50 cm^3/s, and a holding pressure of 800 bar. To isolate the influence of talc, all the process parameters were held constant.

Characterization

An analysis of the crystallization of the PP composites was performed in a Netzsch 200F3 Maia differential scanning calorimeter. Indium, zinc, lead, bismuth, and tin standards were used for temperature calibration. Samples of 18.4 ± 0.5 mg were always cut from the same (middle) position of the injection-molded tensile test specimen. Samples are first heated to 205°C with the rate of 10 K/min, held for 5 min at this temperature to erase the former thermal history, and subsequently cooled with the same speed to room temperature. The data obtained from the DSC cooling cycle were used for the investigation of composite crystallization. Three measurements were performed for every talc concentration, and all the subsequent calculated values are the averages obtained from the three measurements.

To see the influence of specific surface (BET) of the talc with the same chemical structure and d_{50}, two types of Luzenac talcs were compounded with i-PP. The thermal properties of the obtained granulates were investigated using the same DSC program, as in the case of Mondo talc.

Changes in the PP morphology and quality of talc dispersion were visualized using optical light microscopy. Slices of 15–18 μm were prepared using microtome and observed using Axioskop 2 MAT Zeiss equipped with AxioCam MRc with magnification of 500× in all cases.

The agglomeration of talc particles in the composite with 5 and 10 wt % of M30 talc was visualized with computed X-ray tomography (CT). For this purpose, exaCT s50HR computer tomograph was used. The samples with dimensions 10 × 4 × 5 mm were cut from the same tensile bars used for DSC measurements and scanned at 40 kV and 300 mA with an integration time of 0.6 s and a resolution of 16.35 μm. The data were analyzed using the software VG Studio MAX 2.0 and the software tool "defect analysis" with the option "inclusions" and the method "enhanced."

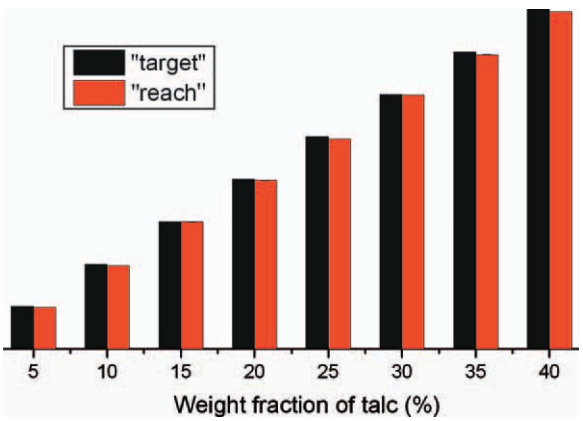

Figure 1 A comparison of the desired and obtained talc concentration after annealing at 600°C for 3.5 h as regards PP filled with Fintalc M05 SLC. [Color figure can be viewed in the online issue, which is available at wileyonlinelibrary.com.]

For the characterization of the crystal structure of PP and the determination of overall degree of crystallinity, we used WAXS analysis. These measurements were carried out on the sliced parts from the middle of the injection-molded samples, using a Siemens D 5005 with Cu Kα radiation of 1.54 Å wavelength at 40 kV and 40 mA. 2θ scan was carried out at a scan speed of 0.6°/min in the 2θ range from 6 to 40°. The samples for WAXS measurements were cut in the same manner as the parts for DSC, and the X-ray beam was set to have a shape and dimensions similar to a cross section of injection-molded parts. In this manner, obtained crystal structure should reflect the average throughout the cross section of the injection-molded parts.

The crystalline long period was measured using a Bruker Nano Star small-angle X-ray scattering (SAXS) with a 2D detector and Cu Kα radiation (45 kV/650 μA). The sample-detector distance was 106.5 cm, and the measurements were conducted in the transmission mode. The samples for SAXS measurements were prepared in the same manner as the parts for WAXS. From the SAXS measurements, long period (D) was calculated and related to the lamellar thickness (l_c) using previously determined crystallinity (X_c) and eq. (11).[36]

$$I_c = D - X_c \tag{11}$$

RESULTS AND DISCUSSION

Mathematical development

Using eq. (10), we attempted to find the influence of talc with different concentrations on the nucleation of i-PP. The result of fitting is presented in Figure 2 for the composite with 5 wt % of Fintalc M05 SLC. Unfortunately, fitting the experimental data into this model did not give the satisfactory linear correlation necessary to find a nucleation parameter K_g, as can be seen from Figure 2. The reason could be the inadequate values of the m and n parameter in Ozawa's model as regards PP/talc composite. During the development of eq. (10), it was assumed that nucleation is instantaneous (thus, parameter n is equal to $m + 1$) and that crystals grow in three dimensions (so the parameter m is equal to 2).

It is obvious that m and n cannot be taken as constants, because they change, due to the influence of talc on nucleation and growth of PP crystals and also do not have to be integer numbers. We thus tried to adapt the eq. (10) to our conditions.

We start from Ozawa model [eq. (7)], which for the case of athermal and instantaneous nucleation [$N(\theta) = \text{const}$] can be written as

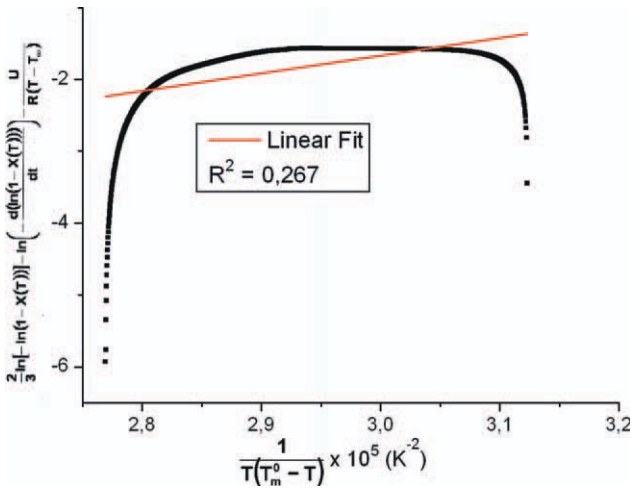

Figure 2 The fitting of the experimental data with eq. (10) for PP filled with 5 wt % of Fintalc M05 SLC. [Color figure can be viewed in the online issue, which is available at wileyonlinelibrary.com.]

$$1 - X(T) = \exp\left[\frac{-gN}{\alpha^n}\int_{T_m^0}^{T}[R(T) - R(\theta)]^m G(\theta)d\theta\right] \tag{12}$$

where

$$R(T) = \int_{T_m^0}^{T} G(\theta)d\theta \tag{13}$$

Thus,

$$1 - X(T) = \exp\left[\frac{-gN}{\alpha^n(m+1)}R(T)^{(m+1)}\right] \tag{14}$$

and

$$\ln(-\ln(1 - X(T))) = \ln\left(\frac{gN}{m+1}\right) - n\ln\alpha + (m+1)\ln R(T) \tag{15}$$

whereas

$$\frac{d(\ln(1 - X(T)))}{dT} = \frac{-gN}{\alpha^n}R(T)^m G(T) \Rightarrow$$
$$\Rightarrow \ln\left(\frac{d(\ln(1 - X(T)))}{dT}\right) = \ln(-gN) - n\ln(\alpha) + m\ln(R(T)) + \ln(G(T)) \tag{16}$$

We now introduce eq. (15) in eq. (16) to obtain logarithm of the spherulite growth rate $\ln[G(T)]$ as follows:

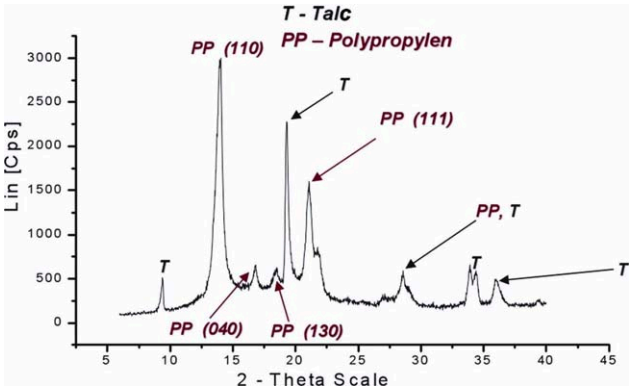

Figure 3 Wide-angle X-ray diffractogram for the PP composite containing 15 wt % of Fintalc M05 SLC. [Color figure can be viewed in the online issue, which is available at wileyonlinelibrary.com.]

$$\ln(G(T)) = \ln\left(\frac{d(\ln(1-X(T)))}{dT}\right) - \frac{m}{m+1}\ln(-\ln(1-X(T))) - \left[\ln(-gN) - \frac{m}{m+1}\ln\left(\frac{gN}{m+1}\right) - \frac{n}{m+1}\ln(\alpha)\right] \quad (17)$$

Because m, g, n, and α are constants for a given talc concentration, eq. (17) can be written in the form:

$$\ln(G(T)) = \ln\left(\frac{d(\ln(1-X(T)))}{dT}\right) - \frac{m}{m+1}\ln(-\ln(1-X(T))) - \phi \quad (18)$$

where ϕ is constant.

We now assume that nonisothermal nucleation with a constant cooling rate could be well approximated with a finite number of isothermal segments. Thus, combining the Lauritzen–Hoffman model for the isothermal case [eqs. (6) and (18)] leads to

$$\ln\left(\frac{d(\ln(1-X(T)))}{dT}\right) - \frac{m}{m+1}\ln(-\ln(1-X(T))) + \frac{U}{R(T-T_\infty)} = [\ln(G_0) + \phi] - \frac{K_g}{T(T_m^0 - T)} \quad (19)$$

We further assume that crystal growth deviates from the pure three-dimensional growth. Concerning this assumption factor, m cannot be taken as a constant, but must be calculated experimentally. The best linear fit of eq. (19) was obtained calculating factor m as $n - 2$ for every talc concentration, where the parameter n was obtained from experimental data using eq. (3) for the nonisothermal case. In this study, the T_g value of PP used was 253 K, $T_\infty = T_g - 30$, $T_m^0 = 481$ K, $U = 6280$ J/mol, and $X(T)$ were obtained from DSC nonisothermal experiments, using eq. (8).

Experimental results

Figure 3 shows an example of WAXS diffractogram of PP containing 15 wt % of talc.

For all talc concentrations, only α-form of i-PP was detected, with characteristic peaks at $2\theta = 14°$, 17°, 18.5°, and 21.5°, as presented in Figure 3. As it can be seen from Figure 3, there is an overlay of PP and talc peaks at about $2\theta = 28.6°$.

An example of the DSC curves for the pure PP and PP filled with different amount of Fintalc M05 SLC is plotted in Figure 4.

As one can see, the onset of crystallization as well as the crystallization peak temperature is shifted to higher temperatures with increasing talc concentration. It follows that talc has a strong nucleation effect, which should be reflected on the structure and size of crystalline units. Contrary to this, only a slight increase is observed in the overall degree of crystallinity, up to a maximum of 5%.

The influence of talc particles on the nucleation of i-PP can be described by the following equation[2]:

$$\Delta G = \Delta G_c \cdot V + A \cdot \sigma_e = (\Delta H - T_c \cdot \Delta S) \cdot V + A \cdot \sigma_e \quad (20)$$

where ΔG_c, ΔH, ΔS, and V are the crystallization free enthalpy, change in enthalpy, entropy, and nuclei volume, respectively. As a consequence from the nucleation activity of the filler, the number of crystallization nuclei that is produced during simultaneous nucleation is increased,[37,28] and the nucleus

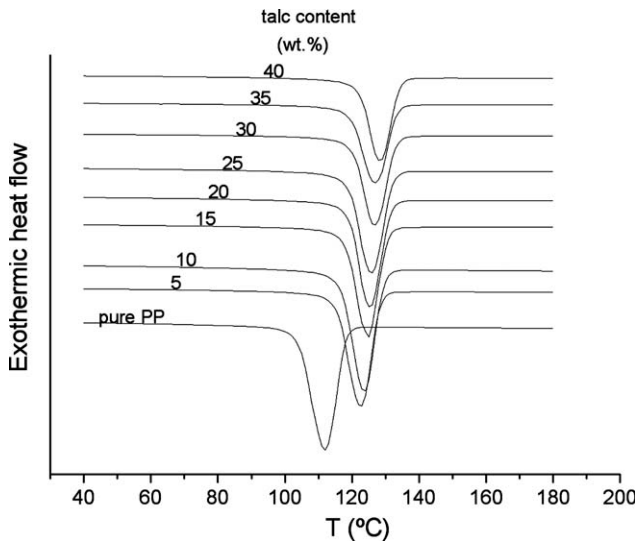

Figure 4 An example of nonisothermal DSC exotherms in pure PP and PP filled with different amounts of Fintalc M05 SLC.

TABLE III
Long Period (D), Overall Degree of Crystallinity (X_c), and Lamellae Thickness (l_c) in Pure PP and in the Composite Containing 10 wt % of Fintalc M05 SLC

Wt % of Talc %)	D (Å)	X_c (–)	l_c (Å)
0	123	0.49	60.3
10	133	0.54	71.8

formation free enthalpy (ΔG) is decreased because of a decrease in fold surface free energy, σ_e.[24,38] As a consequence, the crystallization process starts at a higher temperature (T_c).[27,37,39] The linear growth rate of polymer crystals is a strong function of the degree of undercooling.[a] For smaller undercooling (higher T_c), linear growth is much slower.[28] An increased number of crystallization nuclei, simultaneous nucleation and a lower linear growth rate should give a larger number of thicker and more regular crystals. To prove this, SAXS measurements of pure i-PP were made, as well as PP filled with 10 wt % of Fintalc M05 SLC. Using eq. (11), lamellar thickness is calculated from the long period and presented in Table III. The overall degree of crystallinity (X_c) was obtained from WAXS results using the formula $X_c = P_C/(P_C + P_A + P_T)$, where P_C and P_A are the areas of crystalline and amorphous profile, and P_T is the area of talc peaks.

As expected on the basis of DSC results and theoretical considerations, an introduction of 10 wt % of Fintalc M05 SLC leads to an increase of lamellar thickness from 60.3 Å (in neat PP) to 71.8 Å (in PP filled with 10 wt % of Fintalc M05 SLC). The change in lamellar thickness should have influence on the mechanical properties of materials. This will be discussed in another work.

From the DSC experiments, the time and temperature-dependent relative degrees of crystallinity [$X(t)$ and $X(T)$] were obtained, for every infinitesimal interval, using eqs. (2) and (8), respectively. The baseline used for the integration of DSC heat flow was a straight line crossing the end points. For the approximation of the surface between the DSC heat flow and the constructed baseline, we used a trapezoidal rule. Obtained $X(t)$ and t are used to fit to Avrami's equation [eq. (3)]. Figure 5 shows the fit for PP with 5 wt % of Fintalc M05 SLC with the parameter n as the slope.

It can be observed from Figure 5 that experimental data fit well with Avrami's equation. For every talc concentration, correlation coefficient R^2 was not lower than 0.99. Papageorgiou et al.,[24] found that in the case of PP filled with surface-treated SiO_2 in different concentrations, Avrami's exponent n calculated from nonisothermal DSC measurements was lower than the one for the pure PP at the same cooling rate. In contrast, our investigation demonstrates that in the case of PP filled with talc, n shows the trend of increasing with talc concentration, as presented in Figure 6.

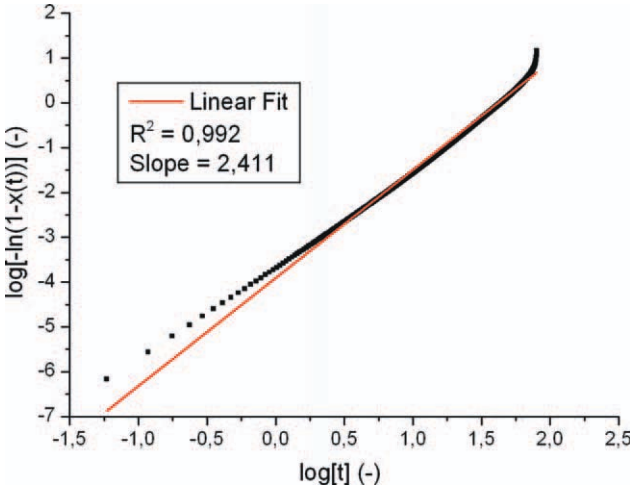

Figure 5 The Avrami plot for PP filled with 5 wt % of Fintalc M05 SLC. [Color figure can be viewed in the online issue, which is available at wileyonlinelibrary.com.]

This trend agrees with the findings of Mucha et al.,[27] while the absolute value of n in the case of pure PP was slightly larger than that obtained by Mucha (2.43 in comparison with 2.16, respectively). Although physical meanings of Avrami's parameters cannot be related to the nonisothermal case in a simple way, the obtained trend of n clearly shows that the nucleation character and dimension of crystal growth change depends on talc concentration. In the future, more attention should be given to defining

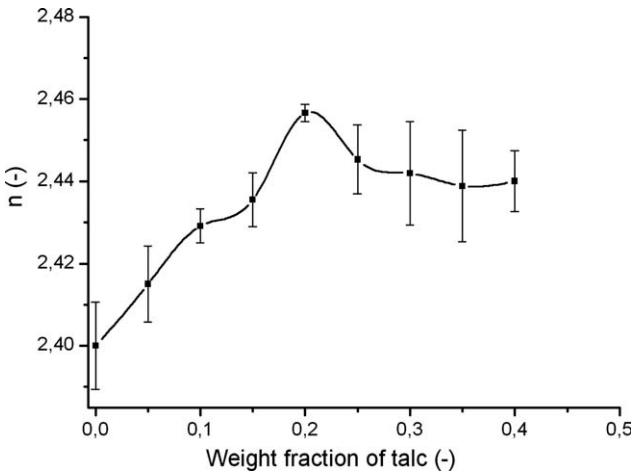

Figure 6 Avrami's exponent n from nonisothermal DSC as a function of Fintalc M05 SLC concentration.

[a]Undercooling is the difference between melting temperature and the onset of crystallization temperature T_c.[30]

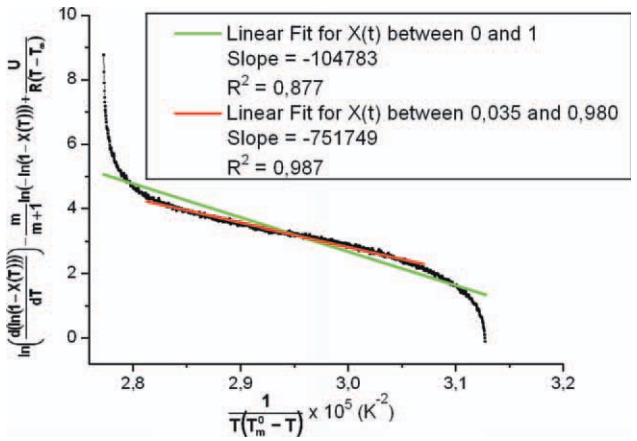

Figure 7 The fitting of the experimental data with eq. (19) for PP fillled with 5 wt % of Fintalc M05 SLC. [Color figure can be viewed in the online issue, which is available at wileyonlinelibrary.com.]

the physical meaning of Avrami's parameter in this case.

The obtained Avrami's parameters n were used to fit eq. (19) with experimental results, and the result of fitting is presented in Figure 7 for PP filled with 5 wt % of Fintalc M05 SLC.

As can be seen, eq. (19) gives satisfactory agreement with experiments, except at the beginning and at the end of the process. The correlation coefficient R^2 was not less than 0.87 in all cases. However, for our further calculations, we used the straight part in Figure 7, which corresponds to the relative degree of conversion between 0.035 and 0.98. K_g values were determined from the slopes and presented in Figure 8.

As can be seen from Figure 8, there is a clear tendency for K_g to decrease as the amount of talc is increased, as a consequence of nucleation activity of talc. After the sharp decrease of K_g between 0 and 5% of talc, there is a plateau up to $\sim$ 20% of talc. Similar behavior obtained in Papageorgiou et al.,[24]

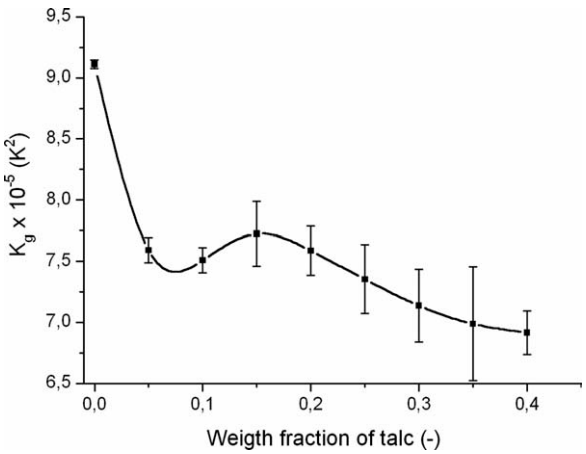

Figure 8 The obtained K_g values in respect to concentration of Fintalc M05 SLC.

where the K_g decrease is almost linear with SiO_2 till 7.7 wt % and then shows a plateau up to 10 wt %. In our case, for the concentrations higher than 20 wt % of talc, K_g further decreases. We assume that when speaking about higher talc concentrations, deagglomeration of talc particles occurs, due to increased shear stress between the numerous particles. To prove this, light microscopy pictures for the pure talc and composites of 5 and 40 wt % were made and presented in Figure 9.

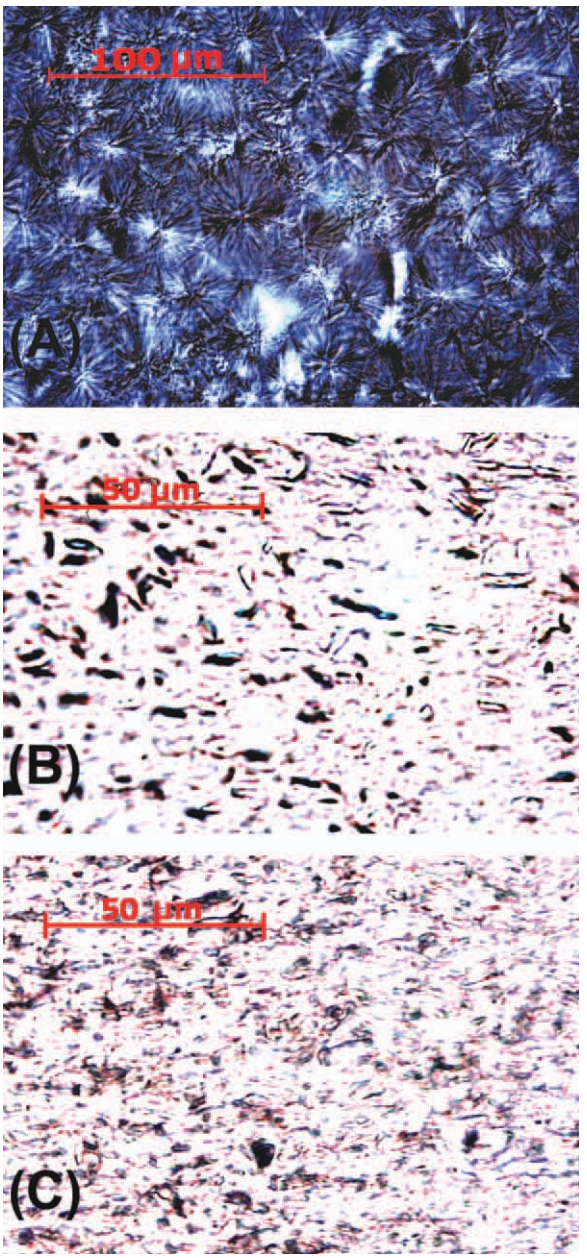

Figure 9 Light microscopy of (**A**) pure PP, (**B**) PP with 5, and (**C**) 40 wt % of Fintalc M05 SLC. The spherulite size in pure PP was between 30 and 40 µm. No spherulitic structure can be seen upon the addition of the talc. [Color figure can be viewed in the online issue, which is available at wileyonlinelibrary.com.]

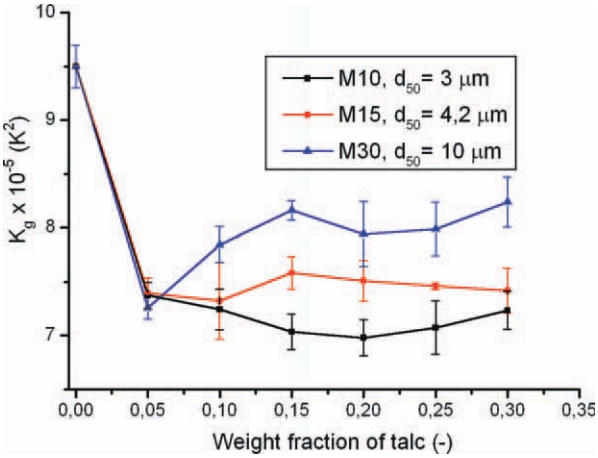

Figure 10 Comparison of nucleation ability of three talc grades with a different d_{50}.[b] [Color figure can be viewed in the online issue, which is available at wileyonlinelibrary.com.]

The comparison between Figure 9(B,C) clearly shows that talc particles were much smaller in the composite with 40 wt % than in the composite with 5 wt % of talc, probably due to the deagglomeration, which happened in the presence of talc in high concentration. This deagglomeration could explain further decrease of K_g for the concentrations higher than 20 wt %, because finer particles are known to be more efficient as nucleation agent.[12]

Using obtained K_g and eq. (5), we calculated the fold surface-free energies (σ_e), and for pure PP, we obtained the value of 0.152 J/m^2. This value was slightly lower than the value obtained by Godovsky and Slonimsky[10] (0.157 J/m^2), using dilatometric measurement. The parameters used in eq. (5) were as follows: $\zeta = 4$; $\sigma = 8.70 \times 10^{-3}$ J/m^2; $b_0 = 0.656$ nm; $\Delta H_f = 134.0$ J/cm^3; $T_m^0 = 481$ K.

Furthermore, we investigated whether it is possible with the new model to see the difference in nucleation ability between three talc grades with different particle sizes. The results are presented in Figure 10.

As expected, the reduction of the energy required for the formation of a nucleus of a critical size is more pronounced for the talc with smaller particles (lower d_{50}), so that the nucleation exponent decreases in the order K_g (M30) > K_g (M15) > K_g (M10). For 5 wt % of talc, there is no observed dependence of K_g on d_{50}. It is possible that for low-talc concentrations, the cooling rate of 10 K/min was too low, so that the homogeneous nucleation takes place at a higher degree; thus, no clear influence of talc particle size is seen. To confirm this assumption, further DSC studies of composites with a lower amount of talc (between 0 and 5 wt %) under a cooling rate higher than 10 K/min are needed.

[b]The Kg value for pure PP in Figure 10 was slightly higher than in Figure 8. The reason could lie in two different batches of PP, which we used for our research.

It is interesting to notice the different trends of K_g in respect to talc concentration between different talc grades presented in Figures 8 and 10. As K_g for example decreases for higher concentrations of M05 SLC talc, a slight increase of K_g was observed in the case of M10 and M30 grades, for the concentrations higher than 20 wt %. It seems that the process does not have the same influence on the dispersion of different talcs. The reason for this could be the different tendencies toward the agglomeration of the talc grades used. It is known that the occurrence and extent of aggregation depend among other factors on the particle size[40,41] and particle size distribution,[41] but the views concerning these effects are contradictory. According to Rumpf,[42] the tensile strength of aggregates depends mainly on the particle size of the filler, and it is increased with decreasing particle diameter. Cheng[43] proposed a different relationship, suggesting a strong dependence between the strength of aggregates and the bulk density of the filler. According to Cheng,[43] the tensile strength of the aggregates should become higher with increasing filler bulk density. On the other hand, it is known that with increasing particle size, the bulk density of the filler increases significantly, indicating strongly increasing tensile strength of the aggregates.[13] In the case when the shear stresses developed in extruder are lower than the aggregate strength, the aggregates remain in the composite, which have an influence on the crystallization behavior of the polymer matrix. It is also not excluded that particle size distribution of the used talc samples changed. Namely, the talc samples used to obtain Figure 10 were stored 7 months before compounding. During this time, segregation of talc is possible according to particle size or particle density. As a consequence, the heavier particles move downward, while the lighter particles remain on the surface. This behavior leads to different particle size distribution within the same talc sample, which could also have an influence on calculated K_g values.

Contrary to other talc grades, a strong increase of K_g occurs between 5 and 10 wt % of M30 talc. Thus, pronounced agglomeration could be expected in the case of 10 wt % of this talc grade. To prove this, samples with 5 and 10 wt % of M30 talc were cut from the same tensile specimens used to obtain Figure 10, and the agglomeration of talc particles was analyzed using CT. The results are presented in Figure 11. As it can be clearly seen from Figure 11, the agglomeration of filler particles as regards 10 wt % occurred to a greater extent compared to the sample with 5 wt % of M30 talc. This was reflected by a higher value of K_g of 10 wt % composite. Although the change in filler particle size due to the agglomeration or deagglomeration, which occurs during the process, has an influence on the behavior of K_g, this complex phenomenon exceeds

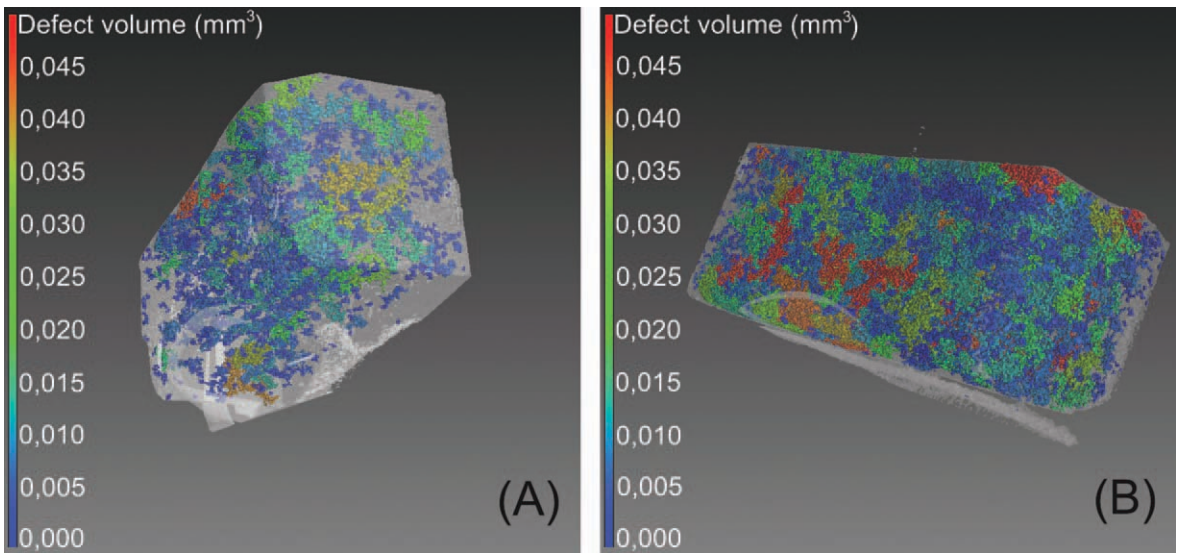

Figure 11 CT images of PP with 5 (**A**) and 10 (**B**) wt % of Fintalc M30. The color of the particles is determined by particle size (red for the coarse and blue for the fine particles). [Color figure can be viewed in the online issue, which is available at wileyonlinelibrary.com.]

the purpose of this article and should be studied in more detail in the future.

We further wanted to examine the difference in nucleation ability of two Luzenac talcs with the same d_{50}, but different specific surface. To find this, we used developed model extension [eq. (19)] and calculated K_g for this two talc grades. HAR T84 talc is produced using an innovative delaminating process. Thus, it possesses a higher aspect ratio and specific surface than conventionally micronized grades, under the same d_{50}. Because of the larger specific surface, the nucleation of the polymer molecules on the HAR T84 should be enhanced, which means that energy required for the formation of a nucleus of a critical size (K_g) should decrease. The results obtained are presented in Figure 12.

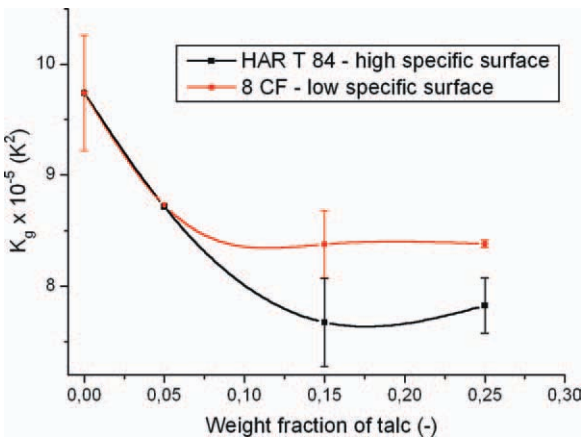

Figure 12 A comparison of the nucleation ability of two Luzenac talcs with the same d_{50} but different-specific surface. [Color figure can be viewed in the online issue, which is available at wileyonlinelibrary.com.]

Indeed, it can be seen that K_g from conventionally produced talc Luzenac 8 CF and delaminated HAR T84 shows the same trend, but, at the same time, Har T 84 possess lower K_g values, which means that this grade shows a higher nucleation ability as regards i-PP.

CONCLUSION

The nonisothermal crystallization of i-PP, nucleated with different talcs, was examined using a novel-proposed extension of the Monasse–Haudin[32] model. The proposed extension seems to be applicable for filled or additive modified semicrystalline polymers and nonisothermal crystallization.

Several conclusions may be proposed:

- A good agreement between the proposed model extension and the literature values was found as regards pure i-PP.
- As expected, a reduction of the nucleation parameter (K_g) with increased talc concentration was found, as a consequence of the talc activity toward nucleation of PP.
- Using the proposed model extension, the comparison between the nucleation activities of three talc types with different particle sizes was made. A good agreement with the predicted trend was obtained. The calculated K_g values decrease with the size of talc particles.
- It was also shown that delaminated talc with a higher specific surface and the same d_{50} provides stronger effect on nucleation of PP compared to the conventionally micronized grade.

- The proposed method proves to be superior to previous approaches regarding filled i-PP under nonisothermal conditions.

Using the proposed model, one can quantify and compare the nucleation effect of different additives in the nonisothermal crystallization of semicrystalline polymers. Starting from the obtained K_g and eq. (5), one can further calculate the fold surface-free energy (σ_e), which is related to the thickness of the secondary nucleus.[23] It remains only to find an adequate model to calculate the thickening of the secondary nucleus in the later stages of crystallization, in order to calculate the final lamellar thickness,[23] which has a great influence on the mechanical behavior of semicrystalline polymers. Therefore, this could be one new way to isolate and study the influence of morphology on the mechanical properties of semicrystalline plastics as well as to establish the mathematical correlations between thermoanalytical methods (DSC measurements), morphology, and the mechanical behavior of polymer materials. This will be addressed in our future manuscript.

The authors thank J. Rudloff for generating the software used for calculation, E. Kraus for performing the CT analysis and S. Götzendörfer for performing WAXS measurements. Helpful discussions with P. Löbmann and G. Sextl are gratefully acknowledged.

References

1. Pasquini, N. Polypropylene Handbook, 2nd ed; Carl Hanser Verlag: München, 2005.
2. Ehrenstein, G. W. Polymeric Materials; Carl Hanser Verlag: München, 2001.
3. Fujiyama, M.; Kitajima, Y.; Inata, H. J Appl Polym Sci 2002, 84, 2142.
4. Sperling, L. H. Introduction to Physical Polymer Science, 3rd ed; Wiley: New York, 2001.
5. Jancar, J. Adv Polym Sci 1999, 139, 1.
6. Gradys, A.; Sejkiewicz, P.; Minakov, A. A.; Adamovsky, S.; Schick, C.; Hashimoto, T.; Saijo, K. Mater Sci Eng 2005, 413, 442.
7. Coccorullo, I.; Pantani, R.; Titomanlio, G. Polymer 2004, 44, 307.
8. Karian, H. G. Handbook of Polypropylene and Polypropylene Composites, 2nd ed; Marcel Dekker: Basel, 2003.
9. Rybnikár, F. J Appl Polym Sci 1982, 27, 1479.
10. Godovsky, Y. K; Slonimsky, G. I. J Polym Sci Polym Phys 1974, 12, 1053.
11. Naiki, M.; Fukui, Y.; Matsumura, T. J Appl Polym Sci 2001, 79, 1693.
12. Ferrage, E.; Martin, F.; Boudet, A.; Petit, S.; Fourty, G.; Jouffret, F.; Micoud, P.; De Parseval, P.; Salvi, S.; Bourgerette, C.; Ferret, J.; Saint-Gerard, Y.; Buratto, S.; Fortune, J. P. J Mater Sci 2002, 37, 1561.
13. Pukánszky, B.; Móczó, J. Macromol Symp 2004, 214, 115.
14. Karger-Kozsis, J. Nano-and Micro-mechanics of Polymer Blends and Composites; Carl Hanser Verlag: München, 2009.
15. Labour, T.; Gauthier, C.; Séguéla, R.; Vigier, G.; Bomal, Y.; Orange, G. Polymer 2001, 42, 7127.
16. Botkin, J. H.; Dunski, N.; Maeder, D. Ciba Speciality Chemicals Inc., Basel, 2002.
17. Kotek, J.; Raab, M.; Baldrian, J.; Grellmann, W. J Appl Polym Sci 2002, 85, 1174.
18. Kotek, J.; Kelnar, I.; Baldrian, J.; Raab, M. Eur Polym J 2004, 40, 679.
19. Raab, M.; Ščudla, J.; Kolarík, J. Eur Polym J 2004, 40, 1317.
20. Zweifel, H. Plastics Additives Handbook, 5th ed; Carl Hanser Verlag: München, 2001.
21. Fujiyama, M.; Wakino, T. J Appl Polym Sci 1991, 42, 2749.
22. Denac, M.; Musil, V.; Šmit, I.; Ranogajec, F. Polym Degrad Stab 2003, 82, 263.
23. Basset, D. C. Principles of Polymer Morphology;University Press: Cambridge, 1981.
24. Papageorgiou, G. Z.; Achilias, D. S.; Bikiaris, D. N.; Karayannidis, G. P. Thermochim Acta 2005, 427, 117.
25. Feng, Y.; Jin, X.; Hay, N. J Appl Polym Sci 1998, 69, 2089.
26. Wunderlich, B. Macromolecular Physics, Vol. 2; Academic Press: New York, 1976.
27. Mucha, M.; Marszalek, J.; Fidrych, A. Polymer 2000, 41, 4137.
28. Cebe, P. Polym Compos 1988, 9, 271.
29. Yiping, H.; Guangmei, C.; Zhen, Y.; Hongwu, L.; Yong, W. Eur Polym J 2005, 41, 2753.
30. Di Lorenzo, M. L.; Silvestre, C. Prog Polym Sci 1999, 24, 917.
31. Hoffman, J. D.; Davis, G. D.; Lauritzen, J. I. In Treatise on Solid State Chemistry, Vol.3; Hannay, N. B., Ed.; Plenum: New York, 1976, Chapter 7.
32. Monasse, B.; Haudin, J. M. Colloid Polym Sci 1986, 264, 117.
33. Ozawa, T. Polymer 1971, 12, 150.
34. Long, Y.; Shankes, R. A.; Stachurski, Z. H. Prog Polym Sci 1995, 20, 651.
35. Housmans, J. W.; Gahleitner, M.; Peters, G. W. M.; Meijer, H. E. H. Polymer 2009, 50, 2304.
36. Tanniru, M.; Misra, R. D. K. Mater Sci Eng A 2005, 405, 178.
37. Fillon, B.; Lotz, B.; Thierry, A.; Wittmann, J. C. J Polym Sci Part B: Polym Phys 1993, 1395.
38. Nagarajan, K.; Levon, K.; Myerson, A. S. J Therm Anal Calorim 2000, 59, 497.
39. Pukánszky, B.; Mudra, I.; Staniek, P. J Vinyl Addit Technol 1997, 3, 53.
40. Pukánszky, B.; Fekete, E. Adv Polym Sci 1999, 139, 109.
41. Fekete, E.; Molnar, Sz.; Kim, G. M.; Michler, G. H.; Pukánszky, B. J Macromol Sci Part B: Polym Phys 1999, B38, 85.
42. Rumpf, H. In Agglomeration;Knepper, W. A., Ed.; Wiley: New York, 1962; p 379.
43. Cheng, D. C. H. Chem Eng Sci 1968, 23, 1405.